Journal of Engineering Mathematics (2005) 51: 35–55

Swimming of the semi-infinite strip revisited

WILLIAM S. VORUS
University of New Orleans, New Orleans, LA, 70148, U.S.A. (wsuna@uno.edu)

Received 29 April 2003; accepted in revised form 17 August 2004

Abstract. Idealized mathematical models have been devised over the years for study of the fundamentals of the swimming of fishes. The two-dimensional flexible strip propelled by execution of transverse traveling-wave undulation is one of the most well-studied of the simple models. This model is redeveloped here, with the finding that higher propulsive efficiencies are theoretically available within the undulatory swimming mode than have been previously exposed. This is by configuring the displacement wave-form for continuously zero circulation over the body length with time, and thereby avoiding the shedding of a vortex wake and its attendant induced drag. The thrust is reactive, via acceleration processes, rather than inductive via relative velocity and lift. As in most of the classical work on fish propulsion, the analysis assumes high Reynolds number and a thin boundary layer, which provides the use of ideal-flow theory. The advance speed is assumed constant and the analysis is initially linearized, but both nonlinear and linear transient analysis are provided in supporting the basic "wakeless swimming" possibility.

Key words: efficiency, hydrodynamics, reduced drag, swimming

1. Introduction

This work is intended to build upon the knowledge provided by a number of classical pioneering works, including [1–5] and particularly [6, 7]. More recent contributions to the field are summarized by Sparenberg [8]. Wu [6, 7] develops mathematics of the waving-strip idealization of fish swimming. This will be the baseline reference called upon here. Appropriate citations of research reported in the intervening years are made in developing the details of this analysis.

The basic assumptions employed in this paper are common to the above references. The main assumption is high Reynolds number, which provides the use of ideal-flow theory. The advance speed is also taken as a time-constant mean value.

Figure 1 below depicts the advancing strip executing traveling-wave oscillation. Here, the coordinate system is translating with speed U_0 in the negative x-direction. The function $h(x,t)$ on Figure 1 is specified as the oscillatory displacement form:

$$h(x,t) = \mathfrak{Re}\left[H(x)\mathrm{e}^{-\mathrm{i}\omega t}\right]. \tag{1}$$

The function $H(x)$ in (1) is the complex amplitude distribution which varies with x, and the undulation is sinusoidal at frequency ω in time. $\mathfrak{Re}$ denotes "real part of" the complex product.

For the element contour function $F = y - h(x,t)$, the kinematic boundary condition that the fluid normal velocity on the contour be equal to the normal contour velocity is:

$$\frac{\mathrm{D}F}{\mathrm{D}t} = 0 \quad \text{on } F(x,t) = 0. \tag{2}$$

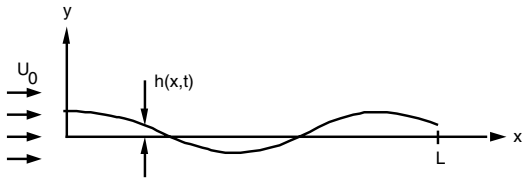

Figure 1. Oscillating strip advancing with speed U_0.

Expansion of (2) gives:

$$h_t(x,t)+(U_0+u)h_x(x,t)=v(x,t) \quad \text{on } y=h(x,t). \tag{3}$$

The subscripts in (3) denote derivatives; $u(x,t)$ and $v(x,t)$ are the horizontal and vertical components of the fluid perturbation velocity on the contour.

2. Linear steady-state analysis

Following [6], assume $h(x,t)/L$ small enough that $u/U_0 \ll 1$ and linearize (3) as:

$$h_t(x,t)+U_0h_x(x,t)=v(x,t) \quad \text{on } y=0;\ 0\le x\le L. \tag{4}$$

The validity of this linearization is addressed in a subsequent section.

2.1. Trivial undulatory mode

To establish a reference for the analysis to follow, consider initially that the amplitude $H(x)$ in (1) is sinusoidal in x with wave length L:

$$H(x)=He^{\frac{2\pi ix}{L}}. \tag{5}$$

The constant H is now the fixed amplitude of the sinusoidal distribution. Substitute (5) in (1) to obtain the sinusoidal traveling wave:

$$h(x,t)=\mathfrak{Re}\left[He^{i(2\pi x/L-\omega t)}\right]. \tag{6}$$

Let $\omega\equiv 2\pi U_0/L$, so that the wave speed is the advance speed. Substitution of (6) in the boundary condition (4) gives the identically zero result:

$$v(x,t)=\mathfrak{Re}\left[2\pi i\left(\frac{H}{L}\right)(U_0-U_0)e^{\frac{2\pi i}{L}(x-U_0t)}\right]\equiv 0. \tag{7}$$

This outcome implies that no disturbance is created by the purely sinusoidal traveling-wave motion of the strip element; there is no pressure developed on the strip, no thrust produced, and no power absorbed. This is, of course, in the absence of viscosity. With zero thrust and ever-present viscous drag, the above conclusion simply implies that a purely sinusoidal traveling-wave form cannot propel itself in a real fluid in that specific motion.

This "perfect" undulatory wave motion, in producing no fluid distrubance, satisfies the condition of minimum work trivially. This conclusion was reached by Wu [6] at the end of his Section 3. Wu's primary interest was in general time dependency. But he assumed that the wave-displacement amplitude $H(x)$ was periodic with fundamental period equal to the strip length L, just as in (5) above. Then, for specialization to harmonic motion in time as well, the result (7) applies to any harmonic in Wu's Fourier cosine expansion of $H(x)$ in L, and

therefore to his general periodic function. Herein lies the major difference in the analysis presented here versus that of Wu. The assumption of periodicity of $H(x)$ in L is concluded to be unnecessarily restrictive, and in fact eliminates a class of aperiodic distributions in $0 \leq x \leq L$ which satisfy the condition of minimum work non-trivially.

The approach is to start from the basis of this time and spatially periodic trivial motion that produces no fluid disturbance at all, and to find a non-trivial disturbance mode that is specified as periodic in time only, and requires minimum, but non-zero work in producing propulsive force.

2.2. A nontrivial undulatory mode

In order for self-propulsion to occur, it is clear that $v(x,t)$ in (4) must be non-zero. For the linear, high-Reynolds-number flow assumed, $v(x,t)$ can be written as the Biot–Savart law in terms of an axis vortex distribution, $\gamma(x,t)$. Equation (4) becomes in this case:

$$h_t(x,t) + U_0 h_x(x,t) = \frac{1}{2\pi}\int_0^L \frac{\gamma(\xi,t)}{x-\xi}\mathrm{d}\xi. \tag{8}$$

Traditional foil theory extends L to infinity in x on the right-hand-side of (8) to allow for the induction due to vortex shedding. This is in the general case where the displacement is an arbitrarily specified function. In such cases, (8) is viewed as an integral equation to be inverted for the vortex strength. In the current analysis, however, which is adopted from the concept presented by Vorus [9], the form of (8) assumes explicitly that no net vorticity is left in the downstream wake of the element. It is consistent with minimum work, since the wake-induced drag is zero. Both quietness and high efficiency would be implied with an eye toward applications.

"Net vorticity" is referred to here as that existing in the real flow process as the non-zero resultant from integration across the shed boundary layer at the foil trailing edge.

In the current development, $h(x,t)$ is the unknown function to be determined from (8) in achieving the condition of no wake, and not $\gamma(x,t)$. However, an additional condition is required on $\gamma(x,t)$: wakeless motion requires that the time rate-of-change of element circulation remain continuously zero. That is, the net circulation of the element, as represented by the integral of γ over the element length, must be zero at all time. This necessary constraint is accomplished with γ specified as periodic in both space and time, with body length L now being some multiple m of the fundamental spatial wave length of the vortex distribution, L/m; m is set to 1 for clarity of the conceptual analysis presented here, but $m > 1$ is easily treated.

The approach is that, instead of $h(x,t)$ being specified as a traveling sinusoidal wave of length L and frequency ω as in the above trivial example of (6) and (7), the vortex distribution is specified as a traveling wave of length L and frequency ω; the wave length of $h(x,t)$ is defined as λ, which is equal to L only for the trivial case represented by (7). The form of the prescribed vortex distribution is therefore:

$$\gamma(x,t) = \Gamma(x)\cos\left(\frac{2\pi x}{L} - \omega t\right) = \Re\mathfrak{e}\left[\Gamma(x)\mathrm{e}^{\mathrm{i}\left(\frac{2\pi x}{L}-\omega t\right)}\right]. \tag{9}$$

The amplitude $\Gamma(x)$ is taken as real but, at this point, as unspecified in (9).

It is convenient to non-dimensionalize the formulation (8) and (9). Define V as the vortex wave speed, or wave phase velocity, vs. the strip translational speed U_0. V is also the speed of the $h(x,t)$ displacement wave. The frequency of the oscillation in (9) is then, by this definition:

$$\omega = 2\pi \frac{V}{L}. \tag{10}$$

Write dimensionless time as $\bar{t} \equiv Vt/L$ and dimensionless $\bar{x} \equiv x/L$, but drop the over-bars for convenience of notation. Consider γ and Γ dimensionless on wave speed V. Equation (9) then takes the form:

$$\gamma(x,t) = \mathfrak{Re}\left\{\Gamma(x)\mathrm{e}^{2\pi \mathrm{i}(x-t)}\right\}. \tag{11}$$

In addition to satisfying the condition that the integral of $\gamma(x,t)$ over the length L be identically zero at all t, the vortex distribution must satisfy the "shockless entry" condition $\gamma(0,t) = 0$ at the leading edge, as well as the "Kutta" condition $\gamma(1,t) = 0$ at the trailing edge. These three conditions are all appropriately satisfied by interpreting $\Gamma(x)$ in (11) as the generalized function:

$$\Gamma(x) = \Gamma\left[H_e(x) - H_e(x-L)\right]. \tag{12}$$

The Heaviside Step Function, $H_e(X)$, is defined as (Lighthill [10, pp. 30–45]):

$$H_e(X) = \begin{matrix} 0 & X < 0 \\ 1 & X \geq 0 \end{matrix}. \tag{13}$$

This treatment of the end-conditions creates a "box function" representation of $\Gamma(x)$ between 0 and 1, with Γ now being an unspecified constant. Multiplication with the traveling-wave exponential in (9), or (11), achieves the continuously zero-lift requirement.

The jump discontinuity at the leading edge by (12) and (13) is a standard specification in steady foil design with the NACA *a*-meanlines. The function (12) places a stagnation point precisely at the leading edge, with a rise in the net tangential velocity amplitude to the constant value of Γ across and immediately downstream of the nose.

The jump in $\Gamma(x)$ at the trailing edge in achieving the Kutta Condition is also a common characteristic specified in steady foil design. The limit of $\Gamma(x)$ as a step at the trailing edge is equivalent conceptually to the well-known and practically very useful constant-pressure, NACA $a = 1$ meanline of steady-foil theory (Newman [11, pp. 175–176]. The physics approximated is high-pressure loading into the trailing edge, but dropping to zero just at the trailing edge, much like the approximation at the leading edge. The $a < 1$ meanlines are often preferred in steady foil design due to concern over trailing-edge separation with the rapidly rising pressure implied. However, with cases of supercavitating or ventilated foils, for example, where separation is not relevant, a rising pressure differential from forward to aft along the foil chord with a jump at the trailing edge is successful in achieving camberlines with the trailing-edge "cupping" necessary for high lift-drag ratio. With unsteady foils, as is the actual case represented by (11), higher tolerance to trailing-edge separation is achieved by the unsteadiness itself, as the surface vorticity is continuously reversing, thereby leaving reduced time in the cycle for premature shedding and separation associated with the high trailing-edge gradient.

The box idealization is a valid theoretical approximation of the edge conditions at this level of analysis, as $\gamma(x,t)$ by (11) is involved only in integration, at (8), and never in differentiation.

Returning to (8), by linearity, one observes that $h(x,t)$ has the periodic form (1) with the same time period, $T = 2\pi/\omega = L/V$, as γ. Substitution of (11) in (8) gives the following first-order linear differential equation for $H(x)$:

$$H_x(x) - \frac{2\pi \mathrm{i}}{U} H(x) = \frac{\Gamma}{U} \Lambda(x), \tag{14}$$

with U being the advance ratio, $U \equiv U_0/V$, by the prescribed non-dimensionalization, and:

$$\Lambda(x) \equiv \frac{1}{2\pi} \int_0^1 \frac{e^{2\pi i\xi}}{x-\xi} d\xi. \tag{15}$$

The solution of (14) is:

$$H(x) = e^{\frac{2\pi i x}{U}} \left(H(0) + \frac{\Gamma}{U} \int_0^x e^{-\frac{2\pi i}{U}\xi} \Lambda(\xi) d\xi \right). \tag{16}$$

In (16), $H(0)$ is the leading-edge displacement amplitude, which has appeared as the constant of integration in the solution. It is noteworthy that, while $\gamma(x,t)$ is periodic in both space and time, by (11), and $h(x,t)$ is periodic in time with the same period as $\gamma(x,t)$, $h(x,t)$ is now *aperiodic* in $0 \le x \le 1$, by (16), with changing undulation amplitude over body length. This is a major departure from Wu's [6,7] assumption of periodicity in $0 \le x \le 1$ and a Fourier series solution in that interval, as noted in the preceding.

Observe that the product of the leading factor in (16) and the $H(0)$ first term in the brackets do represent a sinusoidal wave in x, the amplitude of which is modified over the length of the element, $0 \le x \le 1$, by the second term. The dimensional wave length, λ, of the function is established by the leading factor in (16). It is,

$$\lambda = L\frac{U_0}{V} \tag{17}$$

since in (16) $x = x/L$ and $U = U_0/V$. But the time period, T, of the displacement function is L/V by (10). That is, from (17):

$$T = \frac{L}{V} = \frac{\lambda}{U_0}. \tag{18}$$

The statement of (18) is that "the time required for the strip to advance one wavelength λ at strip speed U_0 is the same as the time required for the wave to advance one strip length L at wave speed V."

Reorganize (18) as:

$$\frac{\lambda}{L} = \frac{U_0}{V}, \quad \text{or non-dimensionally,} \quad \lambda = U; \tag{19}$$

then (19) states that the wavelength ratio is equal to the advance ratio for wakeless swimming. Therefore, the case of wavelength equal to strip length would imply that the wave speed be equal to the advance speed, so that both sides of (19) would be unity; this is the trivial case represented by (7).

$\lambda = U = 1{\cdot}0$ is the zero-slip condition at which no ideal loading is developed and no vortex shedding occurs, but unity ideal efficiency is achieved. This trivial condition is well known in lifting processes, *i.e.*, a "feathering" hydrofoil. The kinematic constraint (19) with $\lambda = U \neq 1{\cdot}0$, might be interpreted as a "weak form" of the zero-slip condition, where non-zero axial load is developed but with necessarily unity ideal efficiency because vortex shedding does not occur. If (19) is not imposed, so that $\lambda \neq U$ such that speed and wavelength are unrelated, then non-zero ideal axial load will be developed, but necessarily accompanied by vortex shedding and reduced ideal efficiency.

2.3. Force considerations

With consideration of viscous skin-friction drag at constant mean non-dimensional advance speed U, the net mean axial force for free-swimming must be zero for force equilibrium. With no lift development, thrust is produced by imparting local aftward acceleration to the fluid particles by body-surface local normal movement. This mechanism of thrust production clearly exhibits ideal-flow hydrodynamics, effectively independent of viscosity [12]. At speed equilibrium in any realization, the mean ideal thrust would be balanced identically by the mean viscous skin-friction resistance developed in the thin, unsteady boundary layer.

Specifically, it is useful to consider the forces developed in terms of fluid momentum considerations, although direct application of the Bernoulli equation produces the same result.

The momentum theorem for a two-dimensional incompressible unsteady flow in the absence of body forces can be written (in dimensional variables):

$$\int\limits_{C_\ell+C_\infty} \vec{\tau}\,\mathrm{d}\ell = \rho \int\limits_{C_\ell+C_\infty} \vec{V}(\vec{V}\cdot\vec{n})\mathrm{d}\ell + \rho \iint\limits_{S} \frac{\partial \vec{V}}{\partial t}\mathrm{d}S. \tag{20}$$

In (20), S is the two-dimensional region bounded externally by the enclosing contour at infinity, C_∞, and internally by, in this case, the element contour C_ℓ. $\vec{n}$ in (20) is the contour unit normal vector, directed out of the fluid. For the ideal flow assumed, the contour stress, $\vec{\tau}$, is the fluid normal pressure $p\vec{n}$. With zero pressure on C_∞, the left-hand side of (20) is the force, $\vec{F}$, on the element.

The first term on the right-hand side of (20) is the flux of momentum across the bounding contours. With continuously zero net circulation about the element as prescribed by (11), there is no net flow acceleration downstream, so that the net momentum flux across C_∞ is zero. With potential flow outside the element contour, (20) reduces to:

$$\vec{F} = \rho \iint\limits_{S} \frac{\partial \vec{\nabla}\phi}{\partial t}\mathrm{d}S + \rho \int\limits_{C_\ell} \vec{\nabla}\phi(\vec{\nabla}\phi\cdot\vec{n})\mathrm{d}\ell. \tag{21}$$

The first term in (21) converts by Gauss' Theorem to produce a contour integral about $C_\ell + C_\infty$. But, with the dipolar-type behavior of the far-field potential and zero net circulation in the domain, the integral over C_∞ is again zero. There results from (21):

$$\vec{F} = \rho \int\limits_{C_\ell} \left[\frac{\partial \phi}{\partial t}\vec{n} + \vec{\nabla}\phi\left(\vec{\nabla}\phi\cdot\vec{n}\right)\right]\mathrm{d}\ell. \tag{22}$$

With reference to Figure 1, on the upper and lower sides of the element contour the unit normal vector is, respectively:

$$\vec{n}^{\pm} = \frac{\pm\left(U_0 h_x \vec{i} - \vec{j}\right)}{\sqrt{1+h_x^2}}. \tag{23}$$

Also on the upper and lower sides of C_ℓ:

$$\vec{V}^{\pm} = \left(U_0 \pm \frac{\gamma}{2}\right)\vec{i} + v^{\pm}\vec{j}. \tag{24}$$

Defining $\Delta\phi \equiv \phi^+ - \phi^-$, (22), with (23) and (24), can be written to first order as an integral over the cut $0 \le x \le L$, $y = 0$ as:

$$\vec{F} = \rho \int_0^L \left[\Delta\phi_t \left(h_x \vec{i} - \vec{j} \right) - U_0 \gamma h_x \vec{i} \right] \mathrm{d}x. \tag{25}$$

The possibility of both transverse and axial force components is displayed in (25).

By definition, the velocity potential jump in (25) is $\Delta\phi(x,t) = -\int \gamma(x,t)\mathrm{d}x$ so that $\Delta\phi_t = -\int \gamma_t \mathrm{d}x$. But by (9), in dimensional variables, $\gamma_t = -V\gamma_x$, where V is the vortex strength wave speed defined at (9). Therefore, $\Delta\phi_t = V\gamma(x,t)$. When this relation is inserted into (25), the element force vector can be written:

$$\vec{F} = \rho\vec{i}(V - U_0) \int_0^L \gamma h_x \mathrm{d}x - \rho\vec{J} \int_0^L \gamma \mathrm{d}x. \tag{26}$$

In dimensionless form, the inviscid vector coefficient of force on the element is then expressed as follows:

$$\vec{C}_f(t) \equiv \frac{\vec{F}(t)}{\frac{1}{2}\rho V^2 L} = 2\vec{i}(1-U) \int_0^1 \gamma(x,t) h_x(x,t)\mathrm{d}x - 2\vec{j} \int_0^1 \gamma(x,t)\mathrm{d}x. \tag{27}$$

The second term above is the y-directed lift, which is zero by (11). The first term is an axial force, which is thrust if positive. Identify the thrust coefficient, which is the first term in (27), as:

$$C_T(t) = 2(1-U) \int_0^1 \gamma(x,t) h_x(x,t)\mathrm{d}x. \tag{28}$$

The leading factor in (28) might be interpreted as a "slip ratio," $1 - U_0/V$; slip in some form is always necessary for thrust production. $U = 1$ in (28) gives zero thrust, and corresponds to the trivial case, (7), where $U_0 = V$ and $\lambda = L$, by (19), as discussed above. The mechanism for "slip" in lift-driven problems is the induction from a vortex wake. Here, with continuously zero circulation there is no wake induction; the slip is an axial slip from the difference in the translational speed U_0 and the wave speed V (19). But it is not immediately clear whether the $1 - U$ factor in (28) is positive or negative for positive thrust production, or whether it can be either, or both.

When the thrust coefficient in the form (28) is considered again, the differential pressure coefficient, by the Bernoulli equation is:

$$C_p(x,t) \equiv \frac{p^+ - p^-}{\frac{1}{2}\rho V^2} = -2(1-U)\gamma(x,t), \tag{29}$$

where $p^+ - p^-$ is the jump in pressure across the strip at (x,t). The thrust coefficient, (28), can therefore be alternatively written, by comparison with (29), as:

$$C_T(t) = -\int_0^1 C_p(x,t) h_x(x,t)\mathrm{d}x \tag{30}$$

A power coefficient corresponding to the input power to the element can also be defined:

$$C_P(t) = \int_0^1 C_p(x,t) h_t(x,t) \mathrm{d}x. \tag{31}$$

From the boundary condition (4), in (31):

$$h_t(x,t) = -U h_x(x,t) + v(x,t) \tag{32}$$

On substituting (32) in (31), with back substitution of (30), there results:

$$C_P = U C_T + \int_0^1 C_p(x,t) v(x,t) \mathrm{d}x = U C_T + C_E(t). \tag{33}$$

The second term on the right in (33) was identified by Wu [6] as the time rate of change of work done on the fluid, or the power dissipated to the fluid, and designated there as $C_E(t) \geq 0$. $C_E(t)$ was, in fact, Wu's objective function in his optimization for high efficiency in Wu [7]. Wu also included a leading-edge suction in his formulation which is not present here because of the absence of circulation; leading-edge suction occurs only with lifting foils and "non-shockless entry".

Now, substitute $v(x,t)$ from the Biot-Savart Law, (8), and $Cp(x,t)$ from (29), in (33) to obtain:

$$C_E(t) = -\frac{1}{\pi}(1-U) \int_{x=0}^1 \int_{\xi=0}^1 \frac{\gamma(x,t)\gamma(\xi,t)}{x-\xi} \mathrm{d}\xi \, \mathrm{d}x. \tag{34}$$

But the integral in (34) is zero by virtue of the symmetry. This can be easily seen by writing the double-integral on the unit-square in (34) alternatively as the sum of the two terms:

$$\int_{x=0}^1 \int_{\xi=x}^1 \frac{\gamma(x,t)\gamma(\xi,t)}{x-\xi} \mathrm{d}\xi \, \mathrm{d}x + \int_{\xi=0}^1 \int_{x=\xi}^1 \frac{\gamma(x,t)\gamma(\xi,t)}{x-\xi} \mathrm{d}\xi \, \mathrm{d}x. \tag{35}$$

Now, reverse the definitions of the x and ξ dummy variables of integration in either of the two integrals in (35) to achieve the zero sum. The clear result in (34) is $C_E = 0$, leaving:

$$C_P(t) = U C_T(t). \tag{36}$$

The definition of Froude propulsive efficiency is output power, or thrust power, over input power. The ideal propulsive efficiency of the element is, by this definition:

$$\eta_i = \frac{U C_T}{C_P}. \tag{37}$$

Substituting (36) in (37): $\eta_i(t) \equiv 1{\cdot}0$, for all values of time.

The result (36) and condition of 100% ideal Froude efficiency that results at (37) is clearly the most important outcome of this work. But it is obviously a necessary outcome in view of the confinement of the vortical flow to the surfaces of the strip by (11) and the elimination of net shed vortex wake and induced drag achieved by (16) via (8) and (11).

Wu [7] establishes $C_E \geq 0$ and states his shape-optimization problem as minimization of C_E under the condition of fixed thrust coefficient. Wu evaluates C_E for various time dependencies

based on his general assumption of periodicity in $0 \leq x \leq 1$. In these evaluations, $C_E > 0$ except for the trivial case of harmonic motion in time, where $C_E = 0$, and $C_T = 0$, corresponding to (7).

The general hydromechanic theory for body thrust generation in ideal fluids without vortex shedding was first suggested by Benjamin and Ellis [13]. This was followed closely by Saffman [12]. Childress [14, pp. 84–87] demonstrates an example of Saffman's theory. Work over the past several decades more firmly establishing the concept includes that of Wu [15], Benjamin and Ellis [16], Miloh [17,18] and, particularly, Miloh and Galper [19]. Essentially, the thrust is inertial, or reactive, and is produced by body accelerations acting through hydrodynamic added mass. This is in contrast to lifting processes where the associated lifting forces and circulation are generated through body and stream relative velocity.

The following quote is from the Introduction of [19]: "It is clear that for self-propulsion phenomena to prevail there must be some mechanism for the exchange of momentum between the body and the fluid." They go on with the development for ideal fluid self-propulsion in terms of momentum transfer from nonlinear body–fluid interaction, rather than the mechanism of vortex shedding. This can be seen in the particular case here in the development of the force vector in formula (28) above. The axial force component is the first term in (26). That term derives entirely from the first term in the momentum theorem, (21), which represents the time rate of change of momentum within the control volume; it is the nonlinear temporal component not involving momentum flux across boundaries, but responsible for momentum exchange none the less. The lift term in (26) is from the momentum flux across the boundaries in terms of the shed vortex wake. But that term is zero since the circulation is zero.

There is then indeed a local fluid motion produced, but it is not rotational motion, and it does not persist to infinity in the ideal fluid. It cancels itself out just downstream. It should be kept in mind that this does not mean there is a zero propulsive power requirement, but only that with no induced wake velocity and attendant induced drag, the propulsive efficiency, (37), is unity. The non-zero local power expenditure achieves the required local momentum exchange. But there is no net dissipative power expended to the fluid, as shown at (33) and (34).

It is appropriate to acknowledge the so-called Sparenberg Theorem, Sparenberg [20], which is stated: "*A body of finite extent, moving periodically in the way as we described, cannot exert a force with non-zero mean value, without shedding vorticity*." But Sparenberg's Theorem [20, pp. 62–63], which is reiterated in Sparenberg [8], requires in its derivation the assumption that the time and spatial periods of the body motion are proportional, with the constant of proportionality being the body translational speed. This proportionality is not a property of the solution developed here in view of (18). Therefore, Sparenberg's Theorem does not apply to this development, except for the special case $U \equiv U_0/V = 1$ in (28), which has been referred to as the "trivial case" at (6) and (7).

2.4. Mean thrust

It is of interest to extract the time-mean thrust from (28). Substitute γ from (11) and $h(x,t)$ from (1) in (28) to obtain:

$$C_T(t) = \Gamma(1-U)\mathfrak{Re}\left\{\int_0^1 H_x(x)\mathrm{e}^{-2\pi \mathrm{i}x}\,\mathrm{d}x + \mathrm{e}^{-4\pi \mathrm{i}t}\int_0^1 H_x(x)\mathrm{e}^{2\pi \mathrm{i}x}\,\mathrm{d}x\right\}. \tag{38}$$

In (38), the first term is time-independent and represents the mean steady propulsive thrust that drives the steady translation of the element. The second, time-dependent term in (38), implies superposition of two cycles of unsteady thrust per cycle of motion on the steady thrust. The physical mechanism of thrust production is clear from (30). The product of $C_p(x,t)$ and $h_x(x,t)$ is an axial elemental force at (x,t) directly related to added mass through the local acceleration. Net thrust requires that the integral of this elemental force distribution be non-zero. Since both C_p and h_x are periodically varying functions of time, their nonlinear product has a mean component, shown in (38). By (38) then, for positive thrust, the slope amplitude $H_x(x)$ must be distributed so that that the net aftward projections of the pressure distribution are larger than the net forward. If $H_x(x)$ is periodic in L, as from (5), the integrand of the steady term in (38) is purely imaginery, resulting in zero mean thrust. With the periodic distribution of $H(x)$, the net forward and aft projections of the pressure distribution are zero in the mean at all times. $U=1$ in (38) then established zero total thrust in the periodic case.

2.5. Displacement prediction

Prediction of the displacement and pressure distributions actually achieved is of interest. Assume the advance ratio U to be specified. There are then two unknown parameters in the displacement amplitude distribution (16): $H(0)$ and Γ. The head amplitude can be eliminated in terms of the total mean thrust coefficient, C_T, which is the first term in (38). By virtue of (36),

$$C_T = \frac{C_P}{U} = 2\pi \frac{\Gamma}{U}(1-U)\Re \mathrm{e}\,\mathrm{i} \int_0^1 H(x)\mathrm{e}^{-2\pi \mathrm{i}x}\mathrm{d}x \tag{39}$$

with C_P from (31). Substitute (16) in (39) and reorganize to achieve:

$$H(0) = \frac{1}{\mathrm{e}^{2\pi \mathrm{i}\frac{1-U}{U}} - 1}\left[\frac{C_T}{\Gamma} - 2\pi \mathrm{i}\frac{1-U}{U}\int_0^1 \mathrm{e}^{2\pi \mathrm{i}\left(\frac{1-U}{U}\right)x}\Delta H(x)\mathrm{d}x\right] \tag{40}$$

with, from (16):

$$\Delta H(x) \equiv \frac{\Gamma}{U}\int_0^x \mathrm{e}^{-\frac{2\pi \mathrm{i}\xi}{U}}\Lambda(\xi)\mathrm{d}\xi. \tag{41}$$

In view of the leading factor in (40), $H(0)$ has infinities at the critical speeds, $U = U_n = 1/n; n = 1, 2, \ldots, \infty$. These critical speeds become clustered in the low-speed range corresponding to large n. On the other hand, nothing has yet eliminated the possibility of displacement distributions that correspond to positive thrust at super-critical speeds $U > 1$. For $U > 1$ in (40) $H(0)$ is not singular, and the production of thrust would be continuous over the super-critical speed range.

The $U_n = 1/n, n \geq 1$, are physically sub-critical advance speeds that cannot occur because thrust production does not occur at these speeds. This is clear from (16):

$$H(x) = \mathrm{e}^{\frac{2\pi \mathrm{i}x}{U}}\left[H(0) + \Delta H(x)\right] \tag{42}$$

with $\Delta H(x)$ by (41). For increasing $H(0)$ as $U \to U_n$ in (42),

$$H(x) \to H(0)\mathrm{e}^{\frac{2\pi \mathrm{i}x}{U_n}} = H(0)\mathrm{e}^{2\pi \mathrm{i}nx}. \tag{43}$$

Equation (43) is a sinusoidal amplitude distribution in $0 \leq x \leq 1$. The frequency of this oscillation is $\omega = \frac{2\pi V}{L}$ by (10), so that with $V = nU_0$ dimensionally, $h_n(x,t)$ is just the nth harmonic of the Fourier series corresponding to the trivial distribution (6), expressed dimensionally as:

$$h_n(x,t) = \mathfrak{Re}\left[H e^{\frac{2\pi i n}{L}(x - U_0 t)} \right] \quad n = 1, 2, \ldots \tag{44}$$

The boundary condition is, just as with (7), satisfied trivially with no disturbance produced by (44). Equation (40), with non-zero Γ, implies that infinite displacement is required to achieve the specified non-zero C_T, which simply means that $C_T = 0$ for finite-head amplitude $H(0)$.

There is no spectrum of the type (41) for the possible supercritical speed range $U > 1$, so that all U would be permitted in (40).

The formulae (16), (40) and (41) give the element displacement amplitude in terms of the single unknown parameter Γ, when U and C_T are assumed to be specified. Γ must be evaluated to proceed further with the analysis. But Γ is not a physically controllable variable, so that some closure condition is needed for uniqueness of the solution. A "minimum displacement" criterion is used here, which determines Γ to minimize the maximum of the modulus of $H(x)$ for specified C_T and U. That is:

$$\Gamma = \Gamma[\min(\mathrm{mod} H(x)_{\max}); C_T, U] \tag{45}$$

with $H(x)$ in terms of Γ by (16), (40), and (41). This condition states that of the family of displacements that give no wake and 100% ideal efficiency, the animal selects the one that requires the minimum maximum displacement. This condition, even if not necessarily a unique condition, is consistent with the achievement of least-work swimming which the animal would be expected to seek. A consideration of energy minimization internal to the animal could be pursued to establish a more rational closure condition, but this is beyond the scope of the current work. Γ was evaluated by the $\min H(x)_{\max}$ criterion using (16), (40), and (41) for varying U and fixed $C_T = 0{\cdot}05$. Figure 2 is a plot of $\min[\mathrm{mod} H(x)_{\max}]$ *vs.* U. The maximum of the pressure coefficient distribution, from (29), is also plotted on Figure 2.

The C_p maximum is relevant to the realism of this analysis from the standpoint of flow separation, particularly with regard to the high negative pressure gradient imposed at the element trailing edge; refer to the preceding argument for the Kutta Condition for the stepped $\gamma(x,t)$ distribution. The instantaneous pressure gradient is proportional to $C_p(x)$ through its relationship to γ, (29). However, it is also relevant that this is an unsteady flow, and therefore has less tendency to separate than a steady flow to which pressure-gradient separation criteria have been developed to apply. The suppression of flow separation in the unsteady process is, of course, due to cyclic vorticity reversals and finite vorticity-diffusion times in the boundary layer of the real unsteady flow process.

The critical speeds corresponding to $U_n = 1/n$, where steady propulsion cannot occur, are clearly evident on Figure 2. It is also clear from Figure 2 that this theory does predict that positive propulsive thrust can be achieved at supercritical $U > 1$. This could be interpreted as forward propulsion with "negative slip," since the wave speed is less than the strip advance speed. The ideal efficiency is unity for all U on Figure 2, but the pressure maximum are larger to propel the strip at increasing U_0 with fixed wave speed, or the converse.

Figure 3a and b shows the displacement distributions calculated from (1), (16), (40), and (45) for two speeds from Figure 2: a subcritical speed $U = 0{\cdot}75$ and a supercritical speed $U = 1{\cdot}25$, with $C_T = 0{\cdot}05$ in both cases. $h(x,t)$ is plotted at two values of dimensionless time for each speed case: $t = 0$ and at the quarter cycle, $t = 0{\cdot}25$.

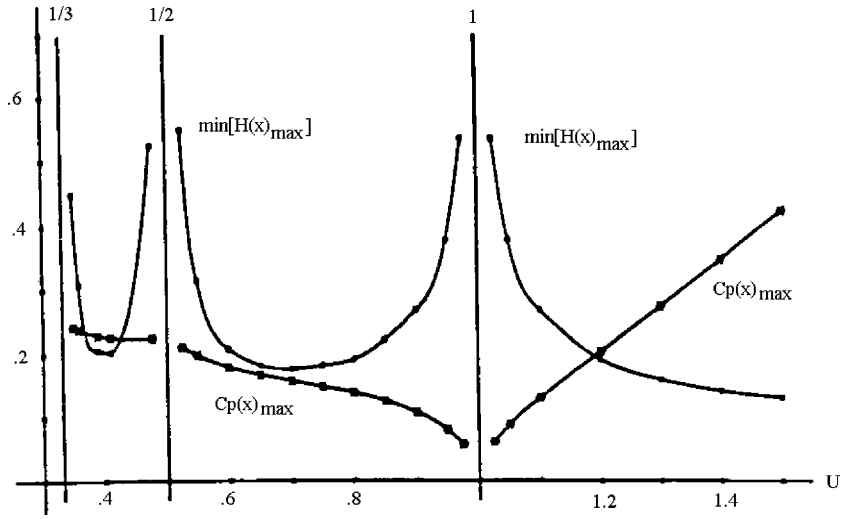

Figure 2. Element displacement and pressure *vs.* speed: $C_T = 0{\cdot}05$.

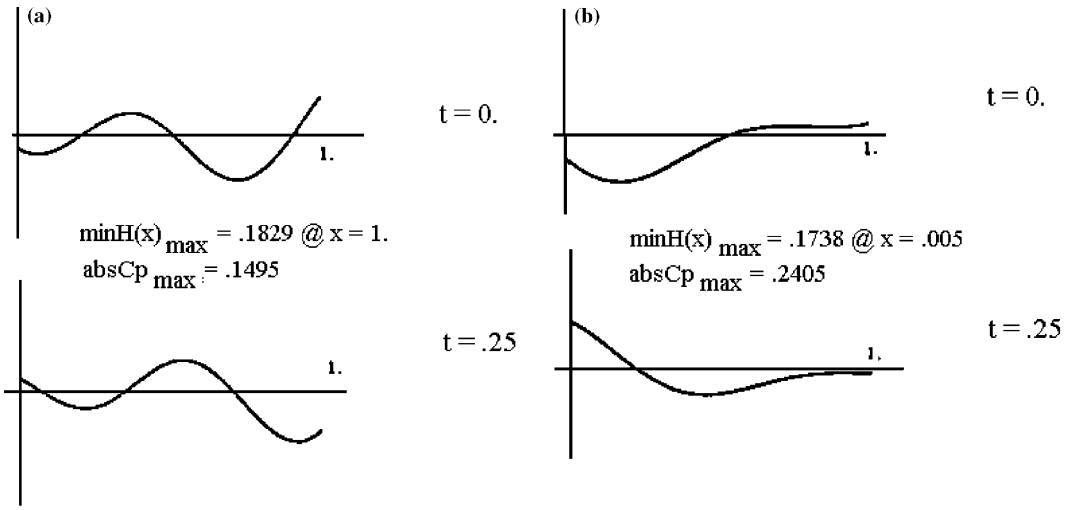

Figure 3. Element displacement *vs.* x (a) $C_T = 0{\cdot}05, U = 0{\cdot}75$; (b) $C_T = 0{\cdot}05, U = 1{\cdot}25$.

The essential point of the demonstration of Figure 3 is that for subcritical speeds the displacement increases toward the tail of the element, and for supercritical speed the displacement decreases toward the tail. Also, with $\lambda = U$, more than one wave length occurs in $0 \leq x \leq 1$ in the subcritical case, and less that one for supercritical speed, *i.e.*, the displacement is more serpentine in the subcritical case, as is clear from Figure 3. This is also seen from the $e^{\frac{2\pi i x}{U}}$ factor appearing in the solution for the $H(x)$ distribution, (16).

Barrett *et al.* [21] concluded that a necessary condition for drag reduction in their tuna-like experimental fish was that the wave phase speed V be larger than the forward speed U_0. That is, they imply the necessity of positive slip, $U < 1$, which is also the most intuitive view. However, that experimental study investigated only wave shapes that increased from head to tail. It is clearly true with the carangiform/tunniform fish that the maximum displacement is at the tail. Their conclusion as to the requirement for positive slip is therefore consistent with the result presented on Figure 3a for the sub-critical case. It does not, however, cover the supercritical speeds where maximum amplitude occurs at the head (Figure 3b).

Some further qualitative relation to animal swimming is possible in view of Figure 3. It is shown by Ayers [22] that the *lamprey* configures its swimming in the sub-critical mode with amplitude increasing toward the tail; λ and $U \approx 0{\cdot}75$ have been observed as typical. It is understood, on the other hand, that the *leach* exhibits the supercritical mode with displacement decreasing toward the tail, as in Figure 3b. Both of these motion shapes are anguilliform. Anguilliform swimming is characterized by large undulating coils over the entire length of the animal body. This is *vs.* carangiform and tunniform swimming, which is characterized more as localized tail flapping. The possibility presented here, with the absence of circulation in this theory, is that steady anguilliform swimming characteristic of the eel family is purely reactive, such that no net vortex wake is left downstream. This conjecture is consistent with the general knowledge of the anguilliform swimmers. In generating thrust without circulation in anguilliform undulation the thrust produced would be second order in the displacement amplitude. The potentially very high efficiency would therefore be achieved at relatively low speed and would require relatively large coils to produce relatively small thrust. This contrasts with carangiform and tunniform fish propulsion, which, although efficient at high speed, is necessarily associated with circulation, and is accompanied by a downstream vortex wake, and associated induced drag, through the pulsating jet generated by the predominant tail motion. The high efficiency in carangiform swimming is achieved by cancellations in the free vortex streams shed from the fish fins, tail, and body; see [21]. In ideal anguilliform swimming, continuous absence of a circulation imbalance would provide that free vortex streams were never created. But the speeds of anguilliform swimmers would have to be less than the carangiform and tunniform, which develop first-order thrusts via lifting processes.

3. Linear time-domain analysis

A time-domain solution as an initial-value problem is of interest both in checking the preceding steady-state frequency domain solution, as well as in providing a base-level model for analysis of more general transient motions. For this purpose the linearized boundary condition (8) can be generalized to:

$$h_t(x,t) + U(t)h_x(x,t) = \frac{1}{2\pi}\int_0^1 \frac{\gamma(\xi,t)}{x-\xi}\mathrm{d}\xi + \frac{1}{2\pi}\int_1^{l(t)} \frac{\gamma_w(\xi,t)}{x-\xi}\mathrm{d}\xi. \tag{46}$$

Here, a shed vortex wake, of strength γ_w, is included to cover the general case and $l(t)$ is the distance from the element trailing edge ($x=1$) to the downstream end of the shed vortex sheet at time t. The start of the motion is from rest, so that $l(0)=0$, with $l(t)$ increasing with time as,

$$l(t) = \int_0^t U(\tau)\mathrm{d}\tau. \tag{47}$$

The use of (46) for the validation purpose here is to consider the vortex distribution as the unknown, to be determined by inverting (46) numerically, for specified $h(x,t)$ as predicted by the foregoing steady-state solution, (1) and (16).

The simple numerical model for solving (46) was constructed as a line of point vortices in the form:

$$\mathrm{RHS}_i^k = \sum_{j=1}^{N+1} C_{ij}^k \lambda_{ij}^k \quad i=1,\ldots,N;\, k=0,1,\ldots \tag{48}$$

In (48), the element has been subdivided into N segments of equal length with point vortices placed at the segment ends. The superscript k in (48) denotes the time step. The terms in (48) are defined as follows:

$$C_{ij} = \tfrac{1}{2\pi}\tfrac{1}{x_i - \xi_j}; \quad \begin{matrix} x_i = (i-1/2)\tfrac{1}{N}, & i = 1, N \\ \xi_j = (j-1)\tfrac{1}{N}, & j = 1, N+1 \end{matrix} \tag{49}$$

$$\mathrm{RHS}_i^k \equiv h_{ti}^{(k)} + U^{(k)} h_{xi}^{(k)} - \sum_{\kappa=0}^{k} C_{i\kappa}\gamma_{w\kappa}^{(k)} \tag{50}$$

The h-derivitives in (50) are available from the solution to the steady-state case for continuously zero circulation, *e.g.*, Figure 3:

$$\begin{aligned} h_{ti}^{(k)} &= -\mathfrak{Re}\left[2\pi \mathrm{i} H(x)\mathrm{e}^{-2\pi \mathrm{i} k\Delta t}\right] \\ h_{xi}^{(k)} &= \mathfrak{Re}\left[H_x(x)\mathrm{e}^{-2\pi \mathrm{i} k\Delta t}\right] \end{aligned} \tag{51}$$

where Δt is the specified time step. Further in (50):

$$C_{i\kappa} = \frac{1}{2\pi}\frac{1}{x_i - (1+\kappa\Delta t)}, \tag{52}$$

$$\gamma_{w\kappa}^{(k)} = \gamma_{w0}^{(k-\kappa)}. \tag{53}$$

The interpretation of (52) and (53) is that shed vortices are left downstream at positions $\xi = 1+\kappa\Delta t$. The strength of the vortex at $1+\kappa\Delta t$ is the value at the trailing edge, $\kappa = 0$, at the time $(k-\kappa)\Delta t$, $\kappa = 0, \ldots, k$. It is to be understood that the initial value $\gamma_{w0}^{(0)} = 0$.

The N algebraic equations (48) are in terms of the $N+1$ unknown vortices. The additional relation required is that the net total circulation at any time (including that of the trailing sheet) remain continuously at the initial value of zero. That is:

$$\sum_{i=1}^{N+1} \varepsilon_i \gamma_i^{(k)} + \sum_{\kappa=0}^{k} \gamma_{w\kappa}^{(k)} = 0, \quad \text{with} \quad \varepsilon_i = \begin{cases} 1 & 1 < i < N+1 \\ 1/2 & i = 0, i = N+1 \end{cases}. \tag{54}$$

The element vortices are from inversion of the linear system (48) and (54) at each time step k. The pressure distribution on the element is then given by (29), assuming $U(t)$ to be a slowly varying, specified, function of time. The force coefficient is from (27), with both the lift and the axial force components retained:

$$\vec{C}_F(t) = C_T(t)\vec{i} + C_L(t)\vec{j} = 2\vec{i}(1-U)\int_0^1 \gamma h_x \mathrm{d}x - 2\vec{j}\int_0^1 \gamma \mathrm{d}x. \tag{55}$$

Figure 4 is a plot of $C_T(t)$ and $C_L(t)$ *vs.* dimensionless time for $U(t)$ varying linearly from 0 to a value of 1·1 at $t = 10$, with $N = 50$. The periodic displacement function $h(x,t)$ in (51) is that of Figure 3a, which is the sub-critical distribution generated for a mean $C_T = 0{\cdot}05$ and constant $U = 0{\cdot}75$.

It is seen from Figure 4 that in the immediate vicinity of the design speed, $U = 0{\cdot}75$, the design steady condition of continuously zero lift (circulation) and non-zero thrust is approximately achieved. Since the sweeping speed U represents a slowly varying transient, precise

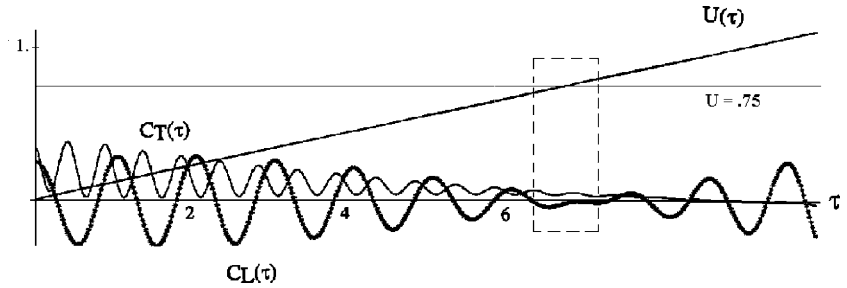

Figure 4. Time-domain solution; speed sweep with displacement distribution set for $\Gamma = 0$ continuously at $U = 0{\cdot}75$.

duplication of the steady-state design case does not occur. Nevertheless, Figure 4 is considered quite supportive of the correctness of the preceding steady-state analysis.

It is noteworthy from Figure 4 that outside of the immediate vicinity of the design speed, the oscillatory lift, with zero mean, becomes relatively large, and, at sub-design speeds, the unsteady thrust has a mean much larger than the steady design thrust. The implication is, in general, that at off-design unsteady swimming, such as starting, changing speeds, or turning, etc., the lift development is accompanied by vortical wake and reduced efficiency. In fact, with an actual anguilliform swimmer, such as an eel, lamprey, or leach, even though it might have the ability for steady "wakeless" swimming, it might be hard to detect even in carefully controlled laboratory experiments. This is because the normal habits of the animal could involve transient swimming most of the time, with the steady, trimmed-out transit pace under study here not so often exercised, and not so easily controlled in the laboratory with live animals.

In fact, direct experimental evidence supporting the conjecture here on "wakeless swimming" has not been found. In this regard, this author can only offer at this time that his interest in anguilliform swimming developed from observation while fishing of a water snake "slithering" through the surfactant field of spring pollen covering the surface of a farm pond. The animal left a very clean and distinct serpentine track of its progression through the pollen, barely wider than the width of its body.

It must be kept in mind that vorticity is always shed at a sharp trailing edge in the real flow in the form of a shed boundary layer that does persist downstream. However, in the absence of the lift asymmetry, the vorticity is an odd function across the wake such that the shed vortex strength, $\gamma(x)$, is zero. This is the requirement for no wake induction in the ideal-flow model and unity ideal Froude efficiency.

4. Nonlinear steady-state analysis

Anguilliform swimming, with which the assumption of reactive thrust without lift has been identified, must be a low-speed, small-thrust, large-amplitude motion. Tail amplitudes as large as 20% of body length have been observed in laboratory studies of lamprey [22]. Linearized theory, based on small displacement, is no doubt applicable for supporting conceptual elucidation, but quantification of the nonlinearity via the boundary condition, (3), requires investigation.

4.1. Analysis

The interest here is in satisfying the boundary condition (3) without the linear reduction to (4). For this purpose, an approximate iteration scheme is implemented based on the linear solution being a good first approximation for the purpose of starting the iteration. The

iteration proceeds by computing the u and v velocities in (3) on the contour h from the previous iterate, and then solving the resulting linear equation for the current iterate contour. The loading, via the specified γ, is retained unchanged over the iteration, as is the case with "inverse-type" formulations where the geometry is the unknown.

Write the kinematic boundary condition (3) for the iteration as:

$$h_t^{(i)}(x,t)+\left\{U+u[x,h^{(i-1)}(x,t),t]\right\}h_x^{(i)}(x,t)=v[x,h^{(i-1)}(x,t),t] \quad \text{on} \quad y=h^{(i-1)}(x,t). \tag{56}$$

Here, the subscript (i) denotes the i^{th} iterate of the element displacement distribution $h(x,t)$, with $h^{(i-1)}(x,t)$ known from the previous iterate, starting with the linear solution: (16), (40), and (45). Equation (56) is then still a linear partial differential equation in terms of its known coefficients and application domain $y=h^{(i-1)}(x,t)$.

With the integration still performed in x, the general field velocities, $u(x,y,t)$ and $v(x,y,t)$, induced by the axis vortex distribution are:

$$u(x,y,t)=-\frac{\Gamma}{2\pi}\,\mathfrak{Re}\left[\mathrm{e}^{-2\pi \mathrm{i}t}\int_0^1[y-h(\xi,t)]\kappa(\xi,y,t)\mathrm{d}\xi\right],$$
$$v(x,y,t)=\frac{\Gamma}{2\pi}\mathfrak{Re}\left[\mathrm{e}^{-2\pi \mathrm{i}t}\int_0^1(x-\xi)\kappa(\xi,y,t)\mathrm{d}\xi\right], \tag{57}$$

with,

$$\kappa(\xi,y,t)\equiv \mathrm{e}^{2\pi \mathrm{i}\xi}\frac{\sqrt{1+h_\xi^2(\xi,t)}}{(x-\xi)^2+[y-h(\xi,t)]^2}$$

where $h(x,t)$ in (57) takes on values of the previous iterate for use in (56) and $y=h^{(i-1)}(x,t)$.

4.2. Solution

For the purpose of reducing the partial differential equation (56) to an ordinary equation in x, consider $U(x,t)$, $v(x,t)$, and $h(x,t)$ to be Fourier-decomposed in time as:

$$u(x,t)=\mathfrak{Re}\sum_{n=0}^{\infty}U_n(x)\mathrm{e}^{-2\pi \mathrm{i}nt}=U_0(x)+\frac{1}{2}\sum_{n=1}^{\infty}\left[U_n(x)\mathrm{e}^{-2\pi \mathrm{i}nt}+\bar{U}_n(x)\mathrm{e}^{2\pi \mathrm{i}nt}\right],$$
$$v(x,t)=\mathfrak{Re}\sum_{m=0}^{\infty}V_m(x)\mathrm{e}^{-2\pi \mathrm{i}mt}, \tag{58}$$
$$h(x,t)=\mathfrak{Re}\sum_{0}^{\infty}H_m(x)\mathrm{e}^{-2\pi \mathrm{i}mt}$$

The over-bar in the first of (58) denotes complex conjugate. In general, the coefficients in the complex Fourier series are, for periodic function $f(t)$:

$$F_m=\frac{\varepsilon}{\pi}\int_t^{2\pi}f(t)\mathrm{e}^{2\pi \mathrm{i}mt}\mathrm{d}t \quad \varepsilon=\begin{cases}1/2 & m=0\\ 1 & m>0\end{cases}. \tag{59}$$

Inserting (58) back in (56) produces:

$$-2\pi\sum_{1}^{\infty} m H_m^{(i)} \mathrm{e}^{-2\pi \mathrm{i} m t} + \left[U + U_0^{(i-1)} + \frac{1}{2}\sum_{n=1}^{\infty}\left(U_n^{(i-1)} \mathrm{e}^{-2\pi \mathrm{i} n t} + \bar{U}_n^{(i-1)} \mathrm{e}^{2\pi \mathrm{i} n t}\right)\right] \times \sum_{m=0}^{\infty} H_{xm}^{(i)}(x) \mathrm{e}^{-2\pi \mathrm{i} m t} = \sum_{m=0}^{\infty} V_m^{(i-1)}(x) \mathrm{e}^{-2\pi \mathrm{i} m t} \tag{60}$$

For the steady $m = 0$ term, (60) reduces to:

$$\left(U + U_0^{(i-1)}\right) H_{x0}^{(i)} + \frac{1}{2}\sum_{m=1}^{\infty} H_{xm}^{(i)} \sum_{m=1}^{\infty} \bar{U}_n^{(i-1)} \mathrm{e}^{2\pi \mathrm{i}(n-m)t} = V_0^{i-1}. \tag{61}$$

This equation can be solved for $H_{x0}^{(i)}(x)$ if $H_{xm}^{(i)}(x)$ is additionally lagged-back one iterate. There results from (61), for $m = 0$:

$$H_{x0}^{(i)}(x) = \frac{1}{U + U_0^{(i-1)}(x)}\left[V_0^{(i-1)}(x) - \frac{1}{2}\sum_{m=1}^{\infty} H_{xm}^{(i-1)}(x) \bar{U}_m^{(i-1)}(x)\right]. \tag{62}$$

For $m > 0$, (61) can be written as the first order differential equation:

$$H_{xm}^{(i)}(x) - \frac{2\pi \mathrm{i} m}{U + U_0^{(i-1)}(x)} H_m^{(i)}(x) = R_m^{(i)}(x) \tag{63}$$

with the known right-hand side:

$$R_m^{(i)}(x) \equiv \frac{1}{U + U_0^{(i-1)}(x)}\left[V_m^{(i-1)}(x) - \frac{1}{2} H_{x0}^{(i)}(x) \bar{U}_m^{(i-1)}(x) - \frac{1}{2}\sum_{l=1}^{\infty} H_{xl}^{(i-1)}(x) \bar{U}_{l-m}^{(i-1)}(x)\right]. \tag{64}$$

The solution of (64) is:

$$H_m^{(i)}(x) = \frac{1}{p_m^{(i)}(x)}\left[H_m^{(i)}(0) + \int_0^x p_m^{(i)}(\xi) R_m^{(i)}(\xi) \mathrm{d}\xi\right], \tag{65}$$

where $p_m^{(i)}(x)$ is the integrating factor:

$$p_m^{(i)}(x) = \mathrm{e}^{\frac{-2\pi \mathrm{i} m}{U}} \int_0^x \frac{\mathrm{d}\xi}{1 + U_0^{(i-1)}(\xi)/U} \tag{66}$$

where $H_m^{(i)}(0)$ in (65) is taken as the value determined for the first iterate linear solution, (40). Hence:

$$H_m^{(i)}(0) = \begin{cases} H(0) & m = 1 \\ 0 & m \neq 1 \end{cases}. \tag{67}$$

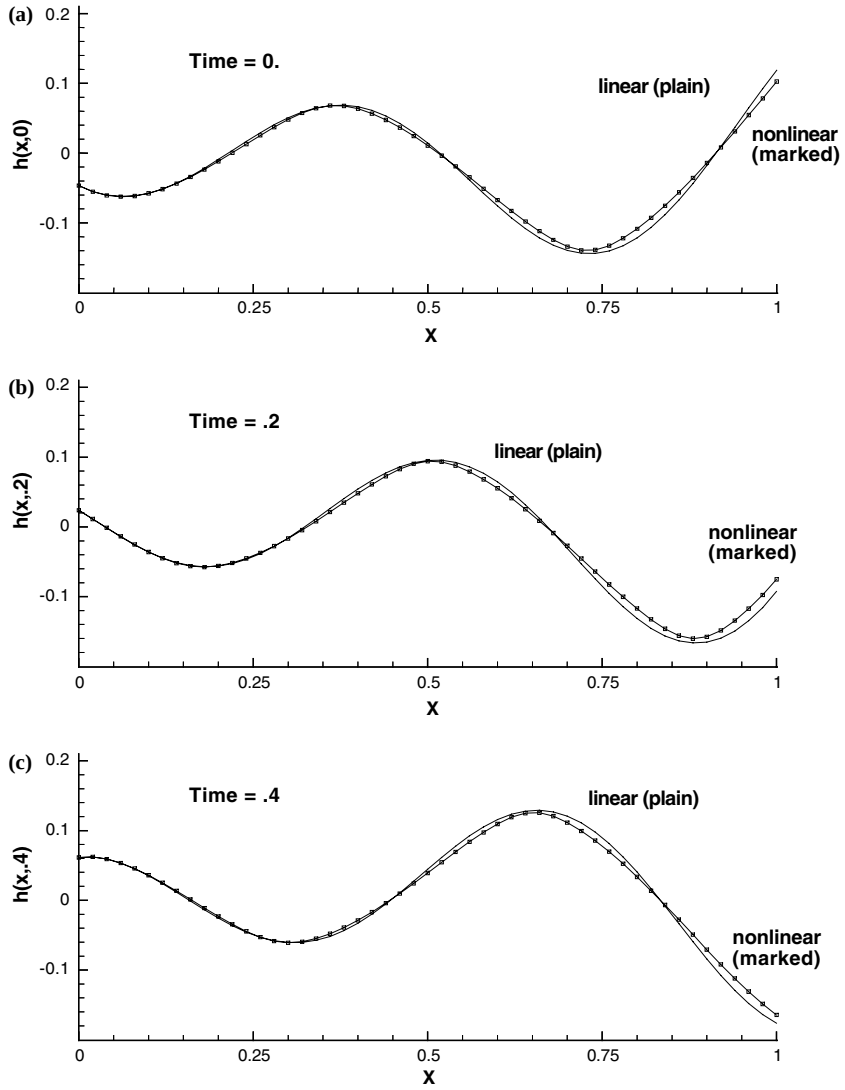

Figure 5. Linear and nonlinear distributions at $CT = 0 \cdot 05, U = 0 \cdot 75$, (for 8 harmonics and 5 iterations): (a) $t = 0$; (b) $t = 0 \cdot 2$; (c) $t = 0{\cdot}4$.

4.3. Calculations

The sub-critical element of Figure 3a, with $U = 0{\cdot}75$ and $C_T = 0{\cdot}05$, was again used as the subject of study for nonlinear effects via (59) to (67). In computing the nonlinear solution from (65), 8 harmonics (0–7) were used in the respective Fourier series and five iterations were applied in achieving convergence. The x-axis in $0 \leq x \leq 1$ was discretized with 50 elements for the numerical analysis.

Comparison of the displacement distributions is shown in Figures 5a–c. The three comparisons are at the times $t = 0 \cdot 0$, $0 \cdot 2$ and $0 \cdot 4$. The cyclic period is $T = 1$, so that a complete comparison is actually available from first quadrant ($t = 0$–$0{\cdot}25$) information, as with Figure 3.

Figure 5 confirms that the displacement amplitudes are large. Nevertheless, the linear distributions leave little to be desired from the standpoint of minimal effect of large amplitude nonlinearity. This should not be unexpected, as the zero-flow perturbation and loading occurs

with the x-periodic sinusoidal displacement whose amplitude is irrelevant, *i.e.*, (7). The effect of the nonlinearity is in the shape changes from the sinusoidal periodic case, and not in the magnitude of the motion itself.

The loads developed by the element exercising the nonlinear displacement distributions is taken the same as for the linear case. With the same vortex distribution specified, the circulation remains continuously zero, implying zero induced drag and 100% ideal efficiency in the nonlinear case as well.

As to one final note of relevance, the mean axial velocity ratio calculated in the process of the nonlinear solution is 0·994, which is consistent with the absence of a vortical jet-flow downstream of the element.

5. Conclusion

This paper has exposed a new theoretical mode of steady self-propulsion of the semi-infinite waving strip that is predicted to produce thrust with no shed vortical wake and with 100% ideal Froude efficiency. This ideal mode is accompanied by a characteristic constraint relation that states that the displacement wave-length-to-body-length ratio, λ, must be equal the body-velocity-to-wave-velocity ratio, U. But this ratio is not to be equal to unity, *i.e.*, $\lambda = U \neq 1$, for non-zero thrust production. The case $\lambda = U = 1$ is the trivial sinusoidal distribution, where vortex shedding is absent and η_i is still unity, but with zero thrust production. At $\lambda \neq U$ non-zero thrust (or possibly drag) is produced, but with vortex shedding and $\eta_i < 1$. By conventional unsteady lifting-foil analysis, vortex shedding and attendant induction necessarily accompany the production of lift, such that $\eta_i < 1$ always. It is necessary to keep in mind that the non-lifting anguilliform-type undulatory motion developed here is a "pumping" motion, and not a "lifting" motion. The accompanying "slip" is axial, and not transverse as with lifting systems.

Another new result exposed by the present theory is that the velocity slip-ratio U can be either less than or greater than unity for the production of positive thrust. The associated displacement shapes compare favorably, yet qualitatively, to the swimming configurations of the anguilla family; the swimming undulations of the *lamprey* ($U < 1.$) and the *leach* ($U > 1.$) in particular, have been cited. It is clear that that the high-speed tunniform and carangiform fishes develop thrust through lifting processes and there the slip-ratio U is necessarily <1.

It is not the claim of this paper that the anguilliform swimmers necessarily exploit the possibilities that appear for minimizing expended swimming energy. The major focus of this presentation has been to build upon the previous theoretical work on the waving strip, namely that of Wu [6, 7], where steady swimming efficiency is also addressed. The semi-infinite strip hydrodynamics is two-dimensional, and none of the anguilliform animal swimmers would produce flows that exhibit much two-dimensionality (except perhaps in very shallow water at low speeds). The basic elements of the two-dimensional theory presented would, however, be expected to be applicable in three-dimensional with similar outcome. But the theory as developed applies only for straight-line translation at constant advance speed. Functional requirements imposed on the anguilla family by their environment and habits, such as feeding, foraging, pursuing, escaping, etc. may result in a very small percentage of activity spent in transit, steady speed, straight-line swimming. In any mode involving transient movement, which might prevail most of the time, vortex shedding would occur, with resulting induced drag, and reduced efficiency.

On the other hand, when in steady translation, these animals do appear, from casual observation, to slide smoothly and effortlessly with minimal residual disturbance left

downstream. Restating from the preceding, the interest of this author in undulatory aquatic propulsion first developed from his notice, while fishing, of a water snake "slithering" through the surfactant field of spring pollen covering the surface of a farm pond. The animal left a very clean and distinct serpentine track of its progression through the pollen, barely wider than the width of its body.

Whether for one reason or another the anguilliform fishes choose to utilize a possible perfect propulsion mode for transit swimming or not can be viewed as somewhat irrelevant from the engineering, *vs*. biological scientific, point of view. Even though the anguilla may not need perfect propulsion much of the time, there are possible practical implementations, not encumbered by limiting habitual and environmental dictates, where high efficiency and quiet operation at steady speed could be of prime importance. This could be, for example, in AUV hardware technology, where, with limited on-board power supply, the capability for maximizing transit speed and/or range would be most important. The possibility of a low-speed, very quiet propulsion device, *i.e*., a "Wave Drive" for a vessel, involving an undulatory element mounted in a casing and attached under the vessel stern, also comes to mind. Precise design, based on a sound theoretical fluid-mechanics foundation, would be essential for successful development of such applications.

Acknowledgements

This research was initially supported through the University of Michigan under ONR Grant N00014-96-0124, and interfaced later with the DARPA Controlled Biological Systems (CBS) Program through Northeastern University.

References

1. M.J. Lighthill, Note on swimming of slender fish. *J. Fluid Mech.* 9 (1960) 305–317.
2. M.J. Lighthill, Aquatic animal propulsion of high hydrodynamic efficiency. *J. Fluid Mech.* 44 (1970) 263–301.
3. M.J. Lighthill, Large amplitude elongated-body theory for fish locomotion. *Proc. R. Soc. London* B 179 (1971) 125–138.
4. G.I. Taylor, Analysis of the swimming of long and narrow animals. *Proc. R. Soc London* A 214 (1952) 158–183.
5. T.Y. Wu, Swimming of a waving plate. *J. Fluid Mech.* 10 (1961) 321–344.
6. T.Y. Wu, Hydromechanics of swimming propulsion. Part I. Swimming of a two-dimensional flexible plate at variable forward speeds in an inviscid fluid. *J. Fluid Mech.* 46 (1971) 337–355.
7. T.Y. Wu, Hydromechanics of swimming propulsion. Part 2. Some optimum shape problems. *J. Fluid Mech.* 46 (1971) 521–544.
8. J.A. Sparenberg, Survey of the mathematical theory of fish locomotion. *J. Engng. Math.* 44 (2002) 395–448.
9. W.S. Vorus, The concept of a traveling-wave propulsor for high efficiency and low wake signature. In: P. Johnson (ed.), 24th American Towing Tank Conference. Offshore Technology Research Center, Texas A & M University (1995) pp. 179–184.
10. M.J. Lighthill, *Fourier Analysis and Generalised Functions*. Cambridge: Cambridge University Press (1964) 79 pp.
11. J.N. Newman, *Marine Hydrodynamics*. Cambridge, MA: The MIT Press(1977) 402 pp.
12. P.G. Saffman, The self-propulsion of a deformable body in a perfect fluid. *J. Fluid Mech.* 28 (1967) 285–289.
13. T.B. Benjamin and A.T. Ellis, The collapse of cavitation bubbles and the pressure thereby produced against solid boundaries. *Phil. Trans. R. Soc. London* A 260 (1966) 221–240.
14. S. Childress, *Mechanics of Swimming and Flying*. Cambridge: Cambridge University Press (1981) 155 pp.
15. T.Y. Wu, The momentum theorem for a deformable body in perfect fluid. *Shiftstechnik* 23 (1975) 229–232.
16. T.B. Benjamin and A.T. Ellis, Self-propulsion of asymmetrically vibrating bubbles. *J. Fluid Mech.* 212 (1990) 65–80.

17. T. Miloh, Optimal self-propulsion of a deformable prolate spheroid. *J. Ship Res.* 27 (1983) 121–130.
18. T. Miloh, Hydrodynamics self-propulsion of deformable bodies and oscillating bubbles. In: T. Miloh (ed.), *Mathematical Approaches in Hydrodynamics.* Philadelphia: S.I.A.M (1991) pp. 21–36.
19. T. Miloh and A. Galper, Self-propulsion of general deformable shapes in a perfect fluid. *Proc. R. Soc. London* A 442 (1993) 273–299.
20. J.A. Sparenberg, *Hydrodynamic Propulsion and Its Optimization – Analytic Theory*. Dordrecht: Kluwer Academic Publishers (1995) 365 pp.
21. D.S. Barrett, M.S. Triantafyllou, K.P. Yue, M.A. Grosenbaugh and M.J. Wolfgang, Drag reduction in fish-like locomotion. *J. Fluid Mech.* 392 (1999) 183–212.
22. J. Ayers, Desktop motion video for scientific image analysis. *Advanced Imaging.* 7 (1992) 52–55.